Electron-phonon coupling and electron heat capacity of metals under conditions of strong electron-phonon nonequilibrium

Zhibin Lin and Leonid V. Zhigilei*
Department of Materials Science and Engineering, University of Virginia, 395 McCormick Road, Charlottesville, Virginia 22904-4745, USA

Vittorio Celli
Department of Physics, University of Virginia, 382 McCormick Road, Charlottesville, Virginia 22904-4714, USA

(Received 23 August 2007; revised manuscript received 22 December 2007; published 28 February 2008)

The dependence of the strength of the electron-phonon coupling and the electron heat capacity on the electron temperature is investigated for eight representative metals, Al, Cu, Ag, Au, Ni, Pt, W, and Ti, for the conditions of strong electron-phonon nonequilibrium. These conditions are characteristic of metal targets subjected to energetic ion bombardment or short-pulse laser irradiation. Computational analysis based on first-principles electronic structure calculations of the electron density of states predicts large deviations (up to an order of magnitude) from the commonly used approximations of linear temperature dependence of the electron heat capacity and a constant electron-phonon coupling. These thermophysical properties are found to be very sensitive to details of the electronic structure of the material. The strength of the electron-phonon coupling can either increase (Al, Au, Ag, Cu, and W), decrease (Ni and Pt), or exhibit nonmonotonic changes (Ti) with increasing electron temperature. The electron heat capacity can exhibit either positive (Au, Ag, Cu, and W) or negative (Ni and Pt) deviations from the linear temperature dependence. The large variations of the thermophysical properties, revealed in this work for the range of electron temperatures typically realized in femtosecond laser material processing applications, have important implications for quantitative computational analysis of ultrafast processes associated with laser interaction with metals.

DOI: 10.1103/PhysRevB.77.075133 PACS number(s): 79.20.Ds, 61.80.Az, 63.20.K−, 71.20.−b

I. INTRODUCTION

The rapidly growing use of femtosecond lasers in practical applications and fundamental materials research increases the demand for quantitative predictive modeling of the fast and highly nonequilibrium processes induced in the target material by the laser excitation. For metals, theoretical and/or computational studies of laser interactions have widely employed the two-temperature model (TTM) proposed by Anisimov *et al.*[1] The TTM describes the temporal and spatial evolution of the lattice and electron temperatures, T_l and T_e, in the irradiated target by two coupled nonlinear differential equations:

$$C_e(T_e)\frac{\partial T_e}{\partial t} = \nabla[K_e(T_e,T_l)\,\nabla\, T_e] - G(T_e)(T_e - T_l) + S(\vec{r},t), \tag{1}$$

$$C_l(T_l)\frac{\partial T_l}{\partial t} = \nabla[K_l(T_l)\,\nabla\, T_l] + G(T_e)(T_e - T_l), \tag{2}$$

where C and K are the heat capacities and thermal conductivities of the electrons and the lattice as denoted by subscripts e and l, $G(T_e)$ is the electron-phonon coupling factor related to the rate of the energy exchange between the electrons and the lattice, and $S(\vec{r},t)$ is a source term describing the local energy deposition by the laser pulse. The model accounts for the laser excitation of the conduction band electrons and subsequent energy relaxation processes, i.e., the energy transfer from the hot electrons to the lattice vibrations due to the electron-phonon interaction and the electron heat conduction from the irradiated surface to the bulk of the target. In Eq. (2), the term describing the lattice heat conduction is often omitted as it is typically negligible as compared to the electron heat conduction in metals.

The TTM is also used in investigations of high-energy ion bombardment of metal targets,[2,3] with the source term in Eq. (1) accounting for the energy transfer from the incident energetic ion to the electronic excitations within the ion track (electronic energy loss by the ion). The TTM equations, typically formulated in this case in cylindrical coordinates, describe the energy transfer from the excited electrons to the lattice, as well as cooling of the thermal spike region, generated by the passage of the incident ion, due to the electron heat conduction.

Some of the effects and physical processes that are not described by the original TTM can still be included within the general TTM framework. In particular, recent developments include incorporation, through the parameters of TTM, of the description of the surface/grain boundary scattering[4,5] and the energy transfer by ballistic electrons,[6,7] combination of TTM with thermoelasticity equations,[8] as well as an extension of TTM to include a description of the transient nonthermal electron dynamics during and immediately after the femtosecond laser excitation.[9] Moreover, investigations of the microscopic mechanisms of laser-induced phase transformations and changes in the microstructure of the target material have been enabled by the development of hybrid models that combine the classical molecular dynamics (MD) method with TTM.[10–17]

A key issue in the application of the models based on TTM for quantitative description of the kinetics of the en-

ergy redistribution in the irradiated target is the choice of adequate temperature dependent thermophysical properties of the target material included in the TTM equation for the electron temperature [Eq. (1)], namely, the electron-phonon coupling factor, the electron heat capacity, and the heat conductivity. Due to the small heat capacity of the electrons in metals and the finite time needed for the electron-phonon equilibration, irradiation by a short laser pulse can transiently bring the target material to a state of strong electron-lattice nonequilibrium, in which the electron temperature can rise up to tens of thousand Kelvins, comparable to the Fermi energy, while the lattice still remains cold. At such high electron temperatures, the thermophysical properties of the material can be affected by the thermal excitation of the lower band electrons, which, in turn, can be very sensitive to the details of the spectrum of electron excitations specific for each metal. Indeed, it has been shown for Au that in the range of electron temperatures typically realized in femtosecond laser material processing applications, thermal excitation of *d* band electrons, located ~2 eV below the Fermi level, can lead to a significant (up to an order of magnitude) increase in the electron-phonon coupling factor and positive deviations of the electron heat capacity from the commonly used linear dependence on the electron temperature.[18–20] On the other hand, in Ni and Pt, where the Fermi level cuts through the high density of electron states *d* band, the same effect of the thermal excitation of *d* band electrons results in the decrease in the strength of the electron-phonon coupling[21] and negative deviations of the electron heat capacity from the linear temperature dependence.[21,22] Thus, the approximations of a linear temperature dependence of the electron heat capacity and a temperature independent electron-phonon coupling factor, used in most of the current TTM calculations, are inappropriate for the quantitative description of material response to a strong ultrafast laser excitation and should be reconsidered based on the analysis of the electronic structure of a given material.

In this paper, we report the results of a systematic analysis of the connections between the electron density of states (DOS) in the target material and the electron temperature dependence of the electron-phonon coupling and the electron heat capacity. Calculations are performed for eight representative metals (aluminum, copper, silver, gold, nickel, platinum, tungsten, and titanium). The paper is organized as follows. In the next section, the theoretical background and computational methods used in the calculations of the electron heat capacity and the electron-phonon coupling are described. In Sec. III, the results of the calculations of the temperature dependent thermophysical properties of the eight metals are presented, compared to the predictions of the free electron gas (FEG) model, and related to the available experimental data obtained at different levels of laser excitation. A brief summary of the results and a discussion of the implications for realistic modeling of femtosecond pulse laser processing are given in Sec. IV.

II. THEORY AND COMPUTATIONAL METHODS

The effect of the thermal excitation of electrons on the electron heat capacity and electron-phonon coupling in metals is determined by the details of the electron DOS, which defines the spectrum of electron excitations and corresponding contributions to the thermophysical properties. Thus, in this section, the method used in the calculations of the electron DOS is described first, followed by the theoretical analysis of the temperature dependence of the electron heat capacity and electron-phonon coupling. A brief discussion of the electron thermal conductivity is also given for completeness, although more detailed analysis of the electron temperature dependence of this parameter will be addressed in future work.

A. Electronic structure calculations

The electron DOSs of the eight metals discussed in this paper are obtained from the electronic structure calculations performed within the density functional theory, using the Vienna *ab initio* simulation package (VASP).[23] The projector augmented wave potential[24] is used in these calculations and the exchange correlation term is accounted for within the generalized gradient approximation. Only valence electrons are explicitly treated in the calculations, while the more tightly bound electrons are represented as core electrons. The integration over the Brillouin zone is performed using a mesh of $31\times31\times31$ points equally spaced in reciprocal space.[25,26] The equilibrium lattice constants and valence electrons treated for each metal are given in Table I.

B. Electron heat capacity $C_e(T_e)$

The electron heat capacity can be calculated by taking the derivative of the total electron energy density with respect to the electron temperature:[27]

$$C_e(T_e) = \int_{-\infty}^{\infty} \frac{\partial f(\varepsilon,\mu,T_e)}{\partial T_e} g(\varepsilon)\varepsilon d\varepsilon, \tag{3}$$

where $g(\varepsilon)$ is the electron DOS at the energy level ε, μ is the chemical potential at T_e, and $f(\varepsilon,\mu,T_e)$ is the Fermi distribution function, defined as $f(\varepsilon,\mu,T_e)=\{\exp[(\varepsilon-\mu)/k_BT_e]+1\}^{-1}$. At low electron temperatures, the Sommerfeld expansion of the electronic free energy is commonly used, giving a linear temperature dependence of the electron heat capacity: $C_e(T_e)=\gamma T_e$, where γ is the electron heat capacity constant, $\gamma=\pi^2k_B^2g(\varepsilon_F)/3$, defined by the value of the electron DOS at the Fermi level, $g(\varepsilon_F)$. Within the free electron gas model,[27] γ can be further associated with the free electron number density n_e and the Fermi energy ε_F, $\gamma=\pi^2n_ek_B^2/2\varepsilon_F$.

At high electron temperatures, however, the Sommerfeld expansion is not valid and the electron heat capacity should be calculated directly from Eq. (3) using the full spectrum of the density of states and $\partial f/\partial T_e$. The evaluation of $\partial f/\partial T_e$ requires the knowledge of the chemical potential as a function of the electron temperature, $\mu(T_e)$. From the conservation of the total number of electrons, the chemical potential can be obtained by setting the result of the integration of the product of the electron DOS and the Fermi distribution function at T_e over all energy levels to be equal to the total number of electrons N_e,[27]

TABLE I. The valence electrons treated in VASP calculations, the equilibrium lattice constant at $T_l=0$ K used in VASP calculations a_0 (Å), the electron-phonon coupling constant λ, the Debye temperature θ_D (K), (Ref. 47), the value of $\lambda\langle\omega^2\rangle$ estimated using the approximation $\langle\omega^2\rangle \approx \theta_D^2/2$ (meV^2), and the value of $\lambda\langle\omega^2\rangle$ (meV^2) used in Eq. (8) for the calculation of the temperature dependence of the electron-phonon coupling factor. For brevity, here and in the text, $\hbar^2$ and k_B^2 factors are omitted when $\langle\omega^2\rangle$ and $\theta_D^2/2$ are given in energy units.

	Al $3s^2 3p^1$	Ag $4d^{10}5s^1$	Cu $3d^{10}4s^1$	Au $5d^{10}6s^1$	Ni $3d^8 4s^2$	Pt $5d^9 6s^1$	W $5d^4 6s^2$	Ti $3d^2 4s^2$
a_0	4.05	4.16	3.635	4.175	3.53	3.92	3.175	2.886[a]
λ	0.45[b]	0.12[c]	0.13[c]	0.17[b]	0.084[d]	0.66[c]	0.28[e,f]	0.38[e,f]
	0.44[g]		0.14[g]	0.15[c]				
	0.38[f]							
θ_D	428	225	343	165	450	240	400	420
$\lambda\theta_D^2/2$	304.8	22.5	56.6	17.1	62.9	140.6	165.7	247.9
	298.1		60.1	15.1				
	257.4							
$\lambda\langle\omega^2\rangle$	185.9[h]	22.5	29 ± 4[e]	23 ± 4[e]	49.5[h]	142.5[h]	112 ± 15[e]	350 ± 30[e]

[a] $c/a=1.63$.
[b] Reference 49.
[c] Reference 55.
[d] Reference 51.
[e] Reference 58.
[f] Reference 43.
[g] Reference 50.
[h] Obtained from experimental values of G_0 (see the text in Sec. III).

$$N_e = \int_{-\infty}^{\infty} f(\varepsilon, \mu(T_e), T_e) g(\varepsilon) d\varepsilon. \tag{4}$$

The chemical potential, obtained with Eq. (4) for different electron temperatures, can then be used in Eq. (3) to predict the temperature dependence of the electron heat capacity. The results of the calculations of $\mu(T_e)$ and $C_e(T_e)$ are presented for eight different metals and compared with the predictions of the free electron gas model in Sec. III.

C. Electron thermal conductivity

The electron thermal conductivity is related to the electron heat capacity through the Drude model relationship, $K_e(T_e, T_l)=v^2 C_e(T_e)\tau_e(T_e, T_l)/3$,[27] where $\tau_e(T_e, T_l)$ is the total electron scattering time and v^2 is the mean square velocity of the electrons contributing to the electron heat conductivity. At low electron temperatures, v^2 can be approximated as the Fermi velocity squared, v_F^2. The total electron scattering rate is given by the sum of the electron-electron scattering rate, $1/\tau_{e\text{-}e}=AT_e^2$, and the electron-phonon scattering rate, $1/\tau_{e\text{-}ph}=BT_l$: $1/\tau_e=1/\tau_{e\text{-}e}+1/\tau_{e\text{-}ph}=AT_e^2+BT_l$, where A and B are typically assumed to be constants.[18,28] The electron-electron and electron-phonon scattering rates, however, might be sensitive to the spectrum of states available for the scattering processes[27] and the temperature dependences of the scattering rates given above might undergo some modifications at high electron temperatures. Thus, in addition to the deviations of the electron heat capacity from the linear temperature dependence, the electron thermal conductivity described by the Drude model relationship might be affected by the modification of the temperature dependences of the electron-phonon and electron-electron scattering rates.

D. Electron-phonon coupling factor $G(T_e)$

The electron-phonon coupling was first analyzed within the free electron gas model by Kaganov *et al.*[29] It was suggested that the electron-lattice energy exchange rate could be expressed in terms of the electron relaxation times at T_e and T_l. At lattice and electron temperatures much higher than the Debye temperature and $T_e \gg T_l$, the rate of energy transfer from the electrons to the lattice per unit volume can then be expressed as[1,29]

$$\left.\frac{\partial E_e}{\partial t}\right|_{ep} = G(T_l - T_e), \quad G = \frac{\pi^2}{6}\frac{m_e C_s^2 n_e}{\tau(T_e)T_e}, \tag{5}$$

where m_e is the effective electron mass, C_s is the speed of sound, n_e is the number density of the electrons, and $\tau(T_e)$ is the electron relaxation time defined as the electron-phonon scattering time, $\tau_{e\text{-}ph}$, and evaluated under the assumption that the lattice temperature is equal to the electron temperature.[29] The electron-phonon scattering time is proportional to the inverse of the lattice temperature and, under the condition of $T_e=T_l$, $\tau(T_e)\sim 1/T_e$, one gets a constant value of the coupling factor given by Eq. (5).

Although a constant value for the electron-phonon coupling factor is used in most of the current computational and theoretical investigations of short-pulse laser interactions with metals, there is growing experimental evidence suggesting that the applicability of the constant electron-phonon coupling may be limited to low laser intensities (low electron temperatures).[18,30–32] For example, the coupling constant has been used as a fitting parameter to obtain an agreement between the calculated and experimental values of the ablation threshold in Au,[33] whereas empirical or semiempirical $G(T_e)$ dependences have been introduced to provide a good description of experimental electron photoemission data[34] and ablation rates.[35,36] Moreover, the measurements of the electron-phonon coupling constants reported in literature exhibit a broad variation, e.g., from 3.6×10^{17} to 10.5×10^{17} W m^{-3} K^{-1} for Ni,[37–39] that may be, in addition to the differences in the measurement techniques, related to the different levels of laser excitation used in the experiments.

Several approaches have been proposed in order to account for the temperature dependence of the electron-phonon coupling factor. Based on the expression of Kaganov *et al.* for the electron-phonon energy exchange rate, [Eq. (5)], Chen *et al.*[35] introduced a model in which both electron-electron and electron-phonon scattering rates are included in the evaluation of the electron relaxation time, $\tau(T_e)$ in Eq. (5). The electron-electron scattering, indeed, starts to significantly contribute to the total electron scattering rate at high electron temperatures, above $\sim$1 eV. While this contribution directly affects the electron transport properties (thermal and electrical conductivities), the relevance of the electron-electron scattering to the electron-phonon coupling factor is questionable. Similarly, the evaluation of the electron relaxation time $\tau(T_e)$ based on the temperature dependence of the electrical or thermal conductivity[2,40] includes the contribution of electron-electron scattering, and is applicable for the calculation of the electron-phonon coupling only at low electron temperatures.

At high electron temperatures, the thermal excitation of the electrons located below the Fermi level starts to contribute to the rate of the electron-phonon energy exchange, and a quantitative analysis of the electron-phonon coupling should go beyond the free electron gas model and should include the consideration of the electron DOS. A general description of the electron-phonon energy exchange involving arbitrary electron DOS was developed by Allen[41] based on the rate equations for the electron-phonon collisions that characterize the phonon emission and absorption processes. Following Allen's analysis, the rate of the energy exchange between the electrons and the lattice within one unit cell can be expressed as

$$\left.\frac{\partial E_e}{\partial t}\right|_{ep} = \frac{4\pi}{\hbar}\sum_{k,k'}\hbar\omega_Q|M_{kk'}|^2S(k,k')\delta(\varepsilon_k-\varepsilon_{k'}+\hbar\omega_Q), \tag{6}$$

where k and Q denote the electron and phonon quantum numbers, respectively. $M_{kk'}$ is the electron-phonon scattering matrix element that defines the probability of scattering of an electron from the initial state k with energy ε_k to the final state k' with energy $\varepsilon_{k'}$ by a phonon of energy $\hbar\omega_Q$.[42] $S(k,k')=(f_k-f_{k'})n_Q-f_{k'}(1-f_k)$ is the so-called thermal factor, expressing the phonon absorption and emission processes in the electron-phonon scattering in terms of the electron and phonon occupation numbers, f_k and n_Q, respectively (see also the Appendix). Assuming that phonons and electrons can be characterized by distinct electron and lattice temperatures, the occupation numbers can be described by Fermi-Dirac and Bose-Einstein distribution functions, respectively: $f(\varepsilon)=1/\{1+\exp[(\varepsilon-\mu)/k_BT_e]\}$ and $n(\hbar\Omega,T_l)=1/[\exp(\hbar\Omega/k_BT_l)-1]$. Near room temperature, only electron states around the Fermi energy contribute to the scattering processes and Eq. (6) can be rewritten in terms of the Eliashberg spectral function for electron-phonon coupling, $\alpha^2F(\Omega)$, commonly used in the superconductivity theory:[41]

$$\left.\frac{\partial E_e}{\partial t}\right|_{ep} = 2\pi g(\varepsilon_F)\int_0^\infty \alpha^2F(\Omega)(\hbar\Omega)^2[n(\hbar\Omega,T_l) - n(\hbar\Omega,T_e)]d\Omega. \tag{7}$$

Allen further suggested a Taylor expansion of Eq. (7) in terms of $\hbar\Omega/k_BT_e$ and $\hbar\Omega/k_BT_l$ under conditions of $\hbar\Omega \ll k_BT_e$ and $\hbar\Omega \ll k_BT_l$, leading to $\partial E_e/\partial t|_{ep}\approx G_0(T_l-T_e)$, where G_0 is the electron-phonon coupling constant: $G_0=\pi\hbar k_B\lambda\langle\omega^2\rangle g(\varepsilon_F)$. In this expression, $\langle\omega^2\rangle$ is the second moment of the phonon spectrum defined by McMillan,[43] and λ is the electron-phonon mass enhancement parameter[44] defined as the first reciprocal moment of the spectral function, $\alpha^2F(\Omega)$: $\lambda\langle\omega^2\rangle=2\int_0^\infty d\Omega\Omega\alpha^2F(\Omega)$.

For high electron temperatures, it is necessary to take into account the scattering processes of electrons away from the Fermi surface, i.e., the electron energy dependence of the electron-phonon spectral function, $\alpha^2F(\varepsilon,\varepsilon',\Omega)$. Wang *et al.*[18] proposed an approximation of the spectral function based on the assumption that $|M_{kk'}|^2$, when summed over scattering angles, is independent of the electron states, which leads to $\alpha^2F(\varepsilon,\varepsilon',\Omega)=[g(\varepsilon)g(\varepsilon')/g^2(\varepsilon_F)]\alpha^2F(\varepsilon_F,\varepsilon_F,\Omega)$. A simple expression for the temperature dependent electron-phonon coupling factor can then be obtained:

$$G(T_e) = \frac{\pi\hbar k_B\lambda\langle\omega^2\rangle}{g(\varepsilon_F)}\int_{-\infty}^{\infty} g^2(\varepsilon)\left(-\frac{\partial f}{\partial\varepsilon}\right)d\varepsilon. \tag{8}$$

The derivation of Eq. (8) and the related assumptions are discussed in more detail in the Appendix. It is easy to verify that at very low electron temperatures, $-\partial f/\partial\varepsilon$ reduces to a delta function centered on the Fermi level at 0 K, and Eq. (8) reduces to a constant value, recovering the expression for G_0 shown by Allen and given above in this section. At elevated electron temperatures, however, the value of $-\partial f/\partial\varepsilon$ at ε away from ε_F can no longer be neglected, leading to a temperature dependent electron-phonon coupling, $G(T_e)$, as described by Eq. (8).

It should be noted that the assumption of the effective independence of the magnitude of the scattering matrix element on the electron states, adopted by Wang *et al.*, is commonly used for estimation of the phonon-induced contribution to the excited electron decay rate, where the electron-phonon scattering matrix is assumed to be constant and the

spectral function, therefore, could be computed from the phonon density of states, given the fact that the electron scatterings take place close to the Fermi surface.[45] This assumption needs further verification when relative contributions from different bands (p/s and d) undergo significant changes with electron temperature. Another assumption implied in the theoretical approach presented above, as well as in other investigations,[18,19,41] is the neglect of the umklapp process[27] in the electron-phonon scattering. Since the temperature dependence of the electron-phonon coupling in this work is determined based on the experimental value of either $\lambda\langle\omega^2\rangle$ or the electron-phonon coupling constant near the room temperature (see the discussion in Sec. III and Table I), the contribution from the umklapp scattering to the room temperature value of the electron-phonon coupling is implicitly taken into account. Furthermore, it has been shown recently by Petrov[46] that the effect of the umklapp process on the temperature dependence of the electron-phonon coupling in aluminum is relatively weak for temperatures exceeding the Debye temperature.

III. RESULTS

In this section, the temperature dependence of the electron heat capacity and the electron-phonon coupling is investigated for eight representative metals in the range of electron temperatures, typically realized in the ultrafast laser processing applications. The results are grouped according to the characteristics of the electron structure of the metals, namely, (1) aluminum and the free electron gas model; (2) noble metals: silver, copper, and gold; (3) transition metals with almost filled d band: nickel and platinum; and (4) transition metals with less than half-filled d band: tungsten and titanium. All calculations are performed based on the theoretical background presented in Sec. II, with the electron DOS obtained from the VASP calculations.

A. Aluminum and the free electron gas model

The results of the calculations of the electron temperature dependence of the thermophysical properties of aluminum, a metal that has a free-electron-like electronic structure, are discussed first and related to the predictions of the free electron gas model. The electron DOS obtained for aluminum in electronic structure calculations performed with VASP at $T_e=0$ K is shown in Fig. 1(a), along with the DOS for the free electron gas model obtained by fitting the parabolic band dependence of $\varepsilon^{1/2}$ to the DOS of aluminum and assuming that the total number of free electrons is 3. While the DOS of aluminum follows the general trend predicted by the free electron gas model, it also exhibits some detailed structure superimposed on the fitted $\varepsilon^{1/2}$ curve. The deviations of the DOS determined for Al in VASP calculations from the free electron gas model DOS result in a slight divergence between the chemical potentials calculated with Eq. (4) using the two DOS [Fig. 1(b)]. Nevertheless, the overall quantitative agreement in the temperature dependences of the chemical potentials predicted with Al and the free electron gas model DOS is very good.

Similar to the chemical potential, the temperature dependence of the electron heat capacity calculated for Al DOS almost coincides with the one calculated for the free electron gas model DOS [Fig. 1(c)]. Moreover, the results of both calculations obtained with Eq. (3) can be well described by the linear dependence, $C_e=\gamma T_e$, with the theoretical value of the coefficient γ calculated within the free electron gas model using the number density of "free" electrons in aluminum $(3s^23p^1)$, $n_e=3.0$ atom^{-1}, as $\gamma_{th}=\pi^2 n_e k_B^2/2\varepsilon_F=91.2$ J m^{-3} K^{-2}, as shown in Fig. 1(c). Note that the experimental value of the electron heat capacity coefficient given in Ref. 47, $\gamma_{exp}=135$ J m^{-3} K^{-2}, is ~48% higher than the theoretical value, $\gamma_{th}=91.2$ J m^{-3} K^{-2}. This difference in γ can be explained by the fact that the experimental value of γ_{exp} is measured at very low temperatures ranging from 0.1 to 4.0 K,[48] where one needs to consider an additional contribution to the electron heat capacity from the electron-phonon interaction, i.e., $C_e=\gamma_{th}(1+\lambda)T_e$.[44] Taking into account that, for aluminum, $\lambda\sim0.42$ (Table I), the agreement between the theoretical calculations of the electron heat capacity and the low-temperature experimental data is very good.

The calculation of the electron temperature dependence of the electron-phonon coupling is based on Eq. (8) and, apart from the electron DOS, requires the knowledge of $\lambda\langle\omega^2\rangle$ material parameter. In the absence of experimental measurements of $\lambda\langle\omega^2\rangle$ for aluminum, a quantitative estimation can be obtained using the reported calculated and experimental values of λ ranging from 0.38 to 0.45 (Refs. 43, 49, and 50) and the approximation for $\langle\omega^2\rangle\approx\theta_D^2/2$,[43,51] yielding the range of values for $\lambda\langle\omega^2\rangle$ from 257.4 to 304.8 meV^2, as shown in Table I. An alternative approach is to choose $\lambda\langle\omega^2\rangle$ based on the results of experimental measurements of electron-phonon coupling. Using the value of the electron-phonon coupling constant measured for Al in thermoreflectance pump-probe experiments,[52] 2.45×10^{17} W m^{-3} K^{-1}, $G(T_e=300\text{ K})$ in Eq. (8) yields $\lambda\langle\omega^2\rangle=185.9$ meV^2. In this work, the latter value of $\lambda\langle\omega^2\rangle$ is adopted in the calculations of the temperature dependent electron-phonon coupling factor for aluminum.

Figure 1(d) shows the electron-phonon coupling factor $G(T_e)$ for aluminum, together with the result obtained with the free electron gas model DOS. The temperature dependence obtained with the aluminum DOS exhibits a sharp increase for electron temperatures up to 5000 K, followed by a slower increase and saturation at higher temperatures. The increase of the strength of the electron-phonon coupling with electron temperature can be interpreted based on the analysis of the DOS for aluminum in the region around the Fermi energy affected by thermal excitations ($\sim k_B T_e$) [Fig. 1(a)]. In contrast to the free electron gas model DOS, where the density of the states increases monotonically with energy, the value of the aluminum DOS at the Fermi level is smaller than that below the Fermi level. As a result, for aluminum, more excited electrons participate in the electron-phonon scattering processes at higher electron temperatures, leading to an increase of the rate of energy exchange between the electrons and the lattice. Note that the enhancement in the strength of the electron-phonon coupling observed for alumi-

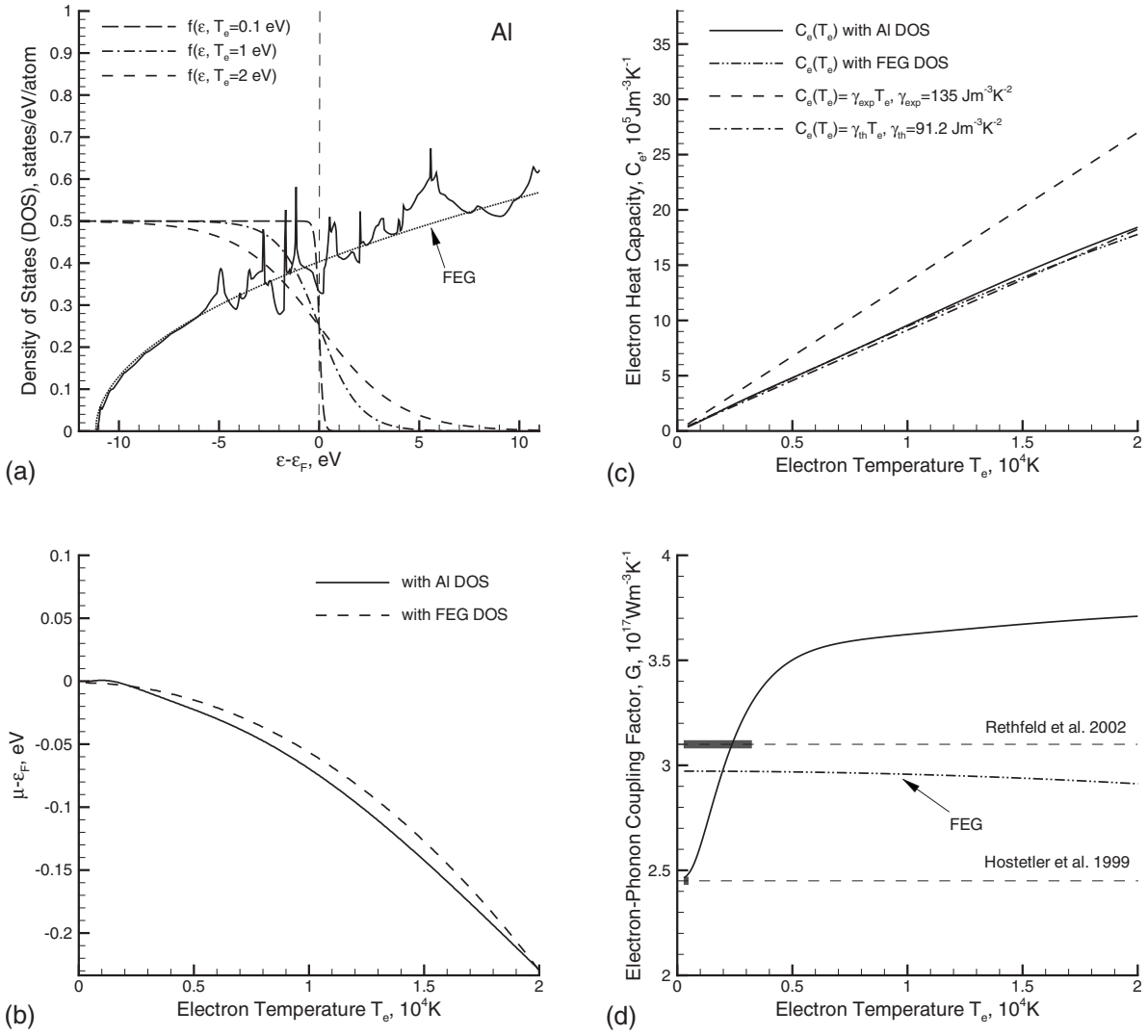

FIG. 1. (a) The electron DOS of aluminum obtained in the electronic structure calculation performed with VASP (solid line), the DOS for the FEG model obtained by fitting $\varepsilon^{1/2}$ dependence to the DOS of aluminum and assuming that the total number of free electrons is 3 (dotted line), and the Fermi distribution function shown for three different values of the electron temperature (dashed and dash-dotted lines). The Fermi distributions are shown centered at the Fermi level at zero temperature. [(b)–(d)] Electron temperature dependence of thermophysical properties of aluminum: (b) the chemical potential, (c) the electron heat capacity, and (d) the electron-phonon coupling factor. Solid lines show the results of the calculations performed with DOS obtained from VASP. Dashed lines in (c) and (d) show the commonly used approximations of the thermophysical material properties based on experimental measurements [(c),(d)] or calculations (d). The ranges of the electron temperature variation in the experiments or calculations used to determine the electron-phonon coupling are shown by bold segments in (d). Dash-dotted lines in (c) and (d) show the predictions of the FEG model. Data presented in this figure are accessible in tabulated form from Ref. 53.

num is relatively small, as compared to other metals considered in this paper (Secs. III B–III D), and reaches ~40% of the room temperature value as the electron temperature increases up to 1×10^4 K.

Contrary to the results for aluminum, the electron-phonon coupling calculated for the free electron gas model DOS slightly decreases with temperature, showing a very weak temperature dependence [Fig. 1(d)]. The calculations are performed with the same value of $\lambda\langle\omega^2\rangle=185.9$ meV^2 as for Al. The difference in the low-temperature values of the electron-phonon coupling between the results obtained for aluminum and the free electron gas model DOS is related to the difference in the values of the two DOS at the Fermi level at 0 K, as can be seen from Fig. 1(a).

Relating the temperature dependence of the electron-phonon coupling predicted for aluminum in this work to the literature values of the electron-phonon coupling constant, one should take into account that the dependence shown in Fig. 1(d) is based on fitting the room temperature value of $G(T_e)$ to $G_0=2.45\times10^{17}$ W m^{-3} K^{-1} measured in thermoreflectance pump-probe experiments performed under conditions when the estimated rise of the electron temperature does not exceed 170 K.[52] A somewhat higher value of 3.1×10^{17} W m^{-3} K^{-1}, obtained in a theoretical analysis of the

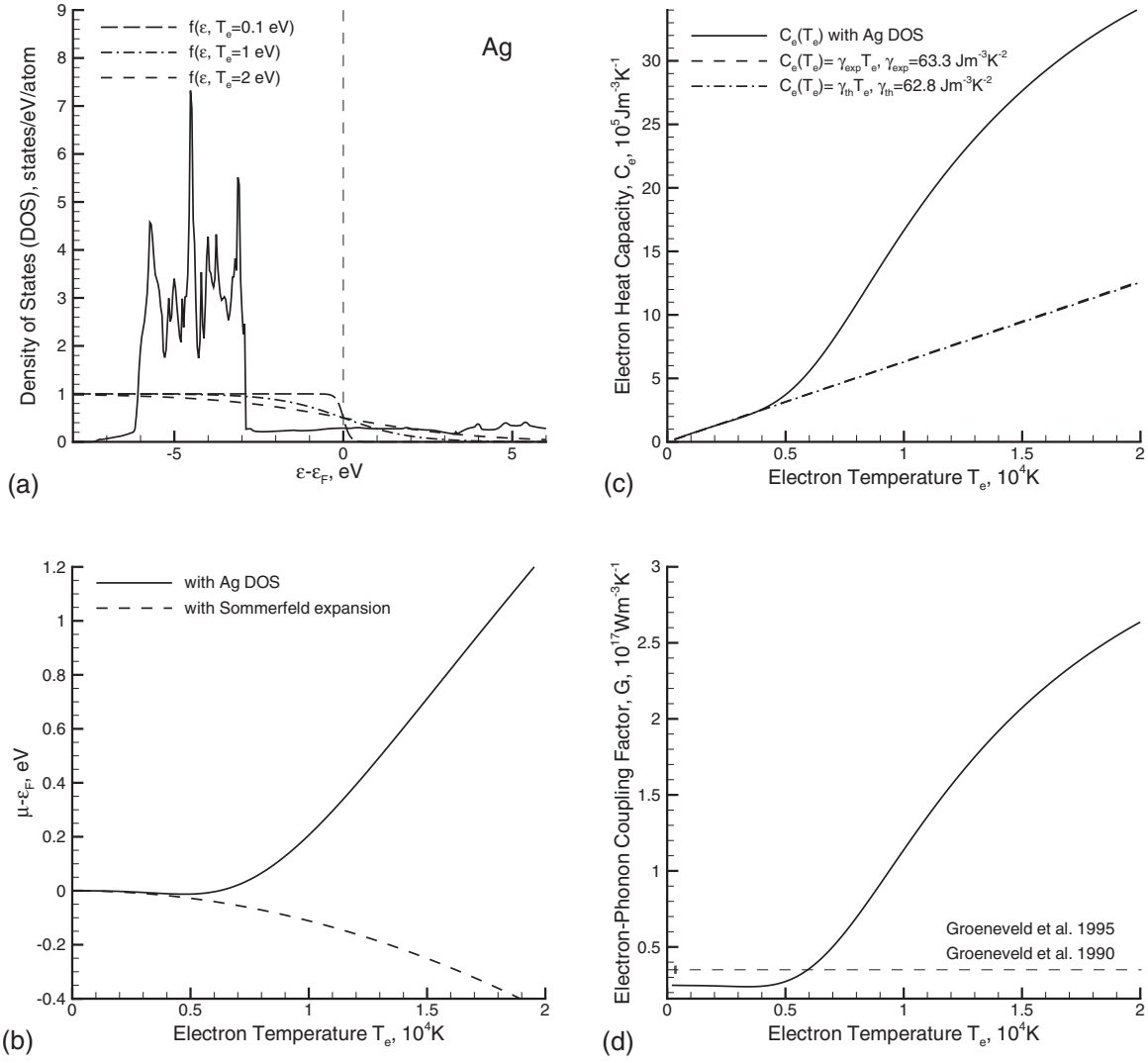

FIG. 2. (a) The electron DOS of silver obtained in the electronic structure calculation performed with VASP (solid line) and the Fermi distribution function shown for three different values of the electron temperature (dashed and dash-dotted lines). The Fermi distributions are shown centered at the Fermi level at zero temperature. [(b)–(d)] Electron temperature dependence of thermophysical properties of silver: (b) the chemical potential, (c) the electron heat capacity, and (d) the electron-phonon coupling factor. Solid lines show the results of the calculations performed with DOS obtained from VASP. Dashed lines in (c) and (d) show the commonly used approximations of the thermophysical material properties based on experimental measurements. The ranges of the electron temperature variation in the experiments used in the measurements of the electron-phonon coupling are shown by bold segments in (d). The dash-dotted line in (c) shows the predictions of the free electron gas model. Data presented in this figure are accessible in tabulated form from Ref. 53.

kinetics of electron-phonon equilibration under conditions of laser excitation leading to $T_e^{max} \sim 3200$ K,[54] is consistent with the predicted temperature dependence.

B. Silver, copper, and gold

The electron DOSs calculated with VASP for three noble metals, silver, copper, and gold [Figs. 2(a), 3(a), and 4(a)], exhibit similar characteristics of the electron band structure. The common feature of the three DOSs is the presence of prominent regions of high density of states, associated with the d bands located $\sim 2-3$ eV below the Fermi level. The mere visual analysis of the DOS together with the Fermi distribution functions, shown in Figs. 2(a), 3(a), and 4(a) for three electron temperatures, suggests that at low electron temperatures, $T_e \sim 0.1$ eV ($\sim 10^3$ K), the region of the electron DOS affected by thermal excitations ($\sim k_B T_e$) is similar to that of the free electron gas model, with only s electrons being excited. At higher electron temperatures, $T_e \sim 1$ eV ($\sim 10^4$ K), a significant number of d band electrons can be excited and can make a substantial contribution to the thermophysical properties of the material. Indeed, at electron temperatures below ~ 5000 K for silver and ~ 3000 K for copper and gold, the calculated chemical potentials [Figs. 2(b), 3(b), and 4(b)] follow the dependence predicted from the Sommerfeld expansion of the electron free energy in the free electron gas model with one free electron per atom. At higher electron temperatures, however, the thermal excitation of electrons from the high density of states edge of the d band to the lower density of states s band results in the

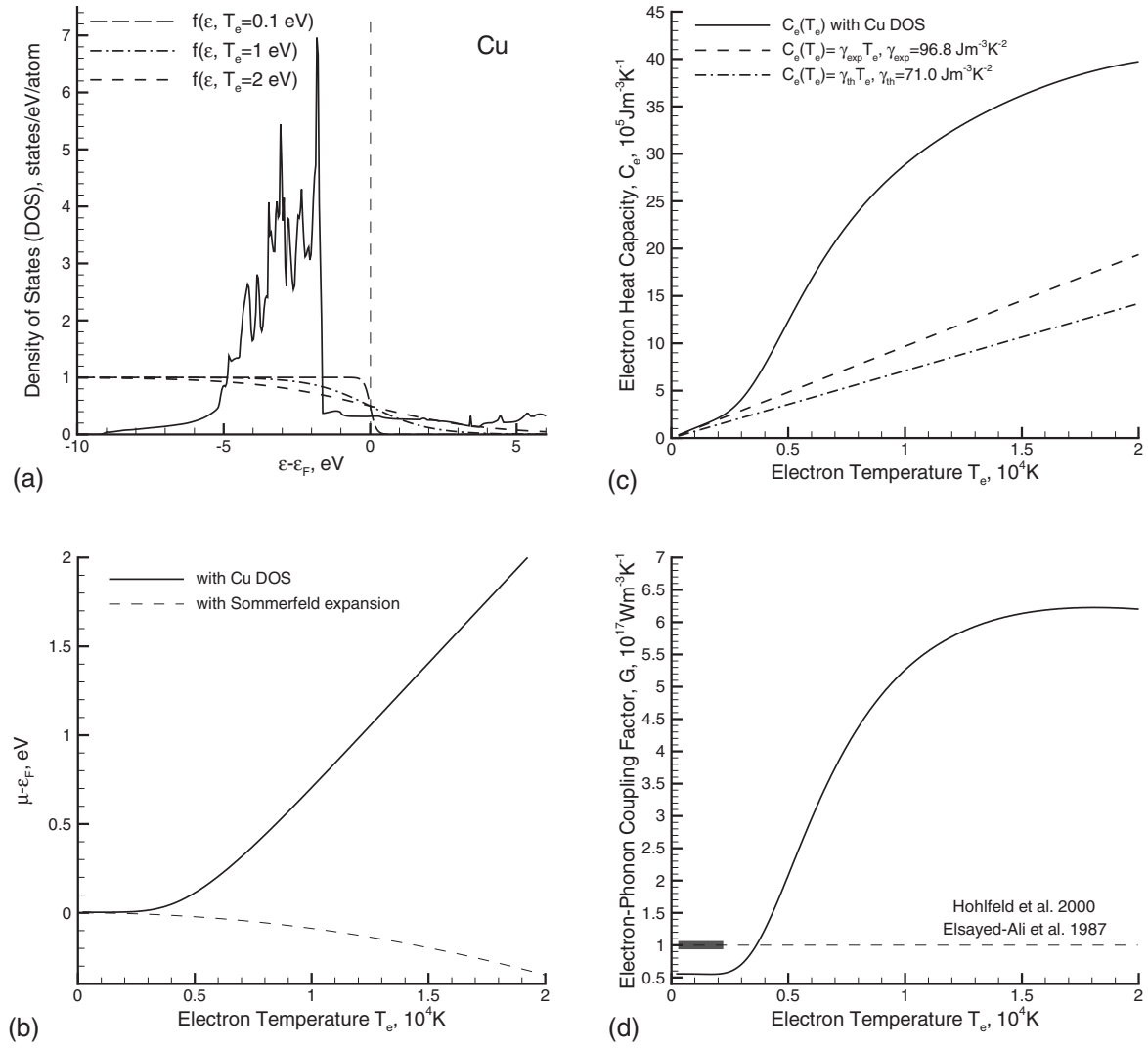

FIG. 3. Same as Fig. 2 but for copper.

increase of the chemical potential and large deviations from the prediction of the free electron gas model.

The results on the electron temperature dependence of the electron heat capacity, $C_e(T_e)$, obtained by incorporating the results for the chemical potential into Eq. (3), are shown for the three noble metals in Figs. 2(c), 3(c), and 4(c). For comparison, the linear dependences, $C_e(T_e)=\gamma T_e$, are plotted for both the low-temperature experimental values of the electron heat capacity coefficient γ_{exp} [63.3 J m^{-3} K^{-2} for Ag, 96.8 J m^{-3} K^{-2} for Cu, and 67.6 J m^{-3} K^{-2} for Au (Ref. 47)], and the theoretical value, calculated as $\gamma_{th}=\pi^2 n_e k_B^2/2\varepsilon_F$ using the number density of s electrons in these noble metals, i.e., $n_e=1.0$ atom^{-1} (62.8 J m^{-3} K^{-2} for Ag, 71.0 J m^{-3} K^{-2} for Cu, and 62.9 J m^{-3} K^{-2} for Au). A better, as compared to Al, agreement between the experimental and theoretical values of the heat capacity coefficients can be attributed to the lower values of the electron-phonon coupling constant λ and Debye temperature θ_D listed in Table I.[44]

At low electron temperatures, below a few thousand Kelvins, the $C_e(T_e)$ dependences predicted by Eq. (3) follow closely the linear dependences plotted with experimental values of the heat capacity coefficients. However, as the electron temperature becomes sufficiently high for thermal excitation of a significant number of d electrons, positive deviations from the linear temperature dependences are observed for all three noble metals. The deviations start at ~3000 K in Cu and Au, where the high-energy edge of the d band is located ~2 eV below the Fermi energy, and at a higher temperature of ~5000 K in Ag, where the d band is located deeper, ~3 eV below the Fermi level. The large deviations of the electron heat capacity from the linear dependence at electron temperatures that are readily achieved in laser material processing applications suggest that the application of the commonly used linear approximation $C_e(T_e)=\gamma T_e$ can result in a significant overestimation of the transient values of the electron temperature during the time of the electron-lattice nonequilibrium. The linear approximation is, therefore, inappropriate for quantitative modeling of the laser-induced processes in noble metals under conditions when the electron temperature exceeds several thousand Kelvins.

The effect of the thermal excitation of d band electrons, discussed above for electron heat capacity, has also strong implications for the temperature dependence of the electron-

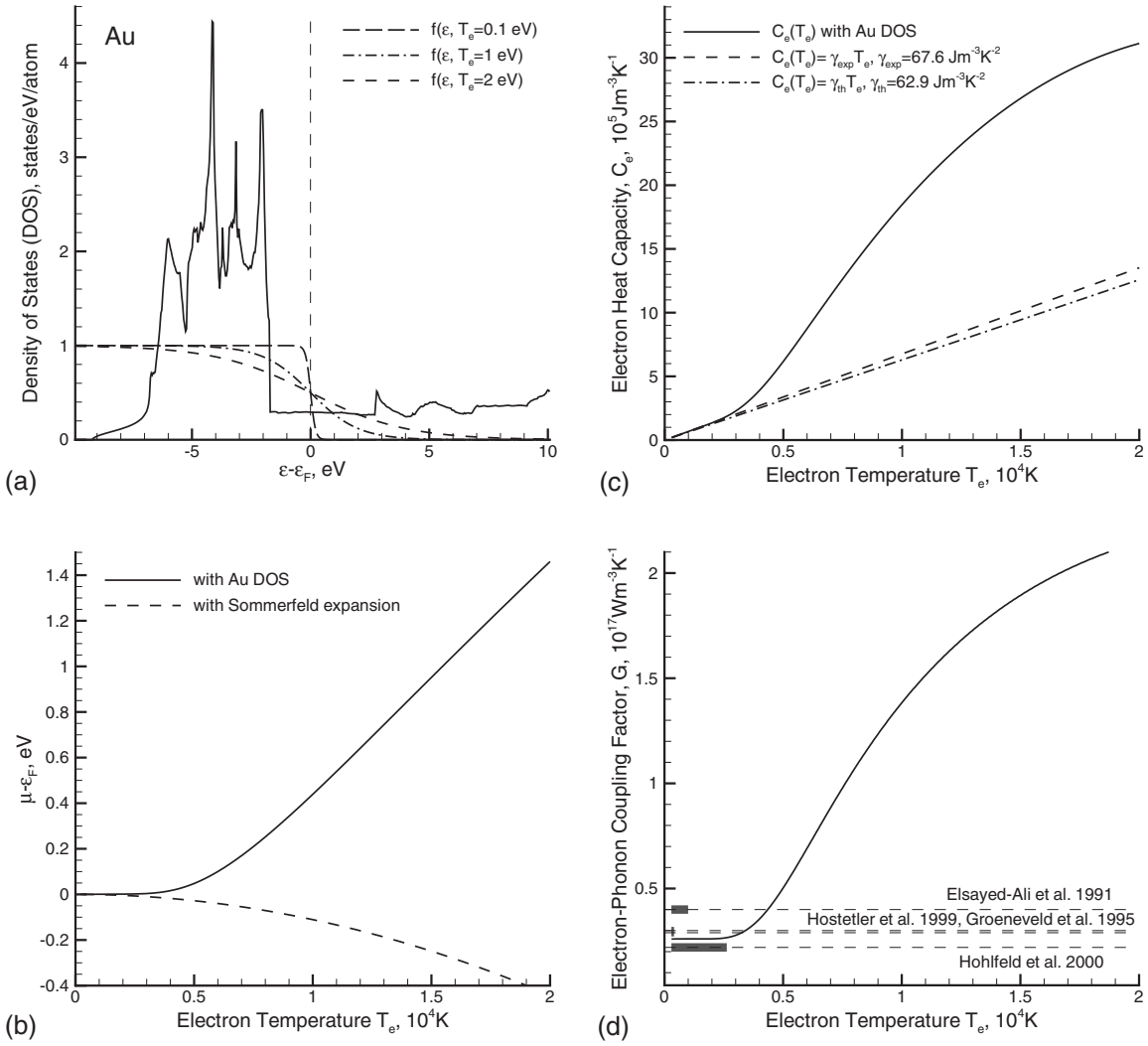

FIG. 4. Same as Fig. 2 but for gold.

phonon coupling $G(T_e)$. The results of the calculations of $G(T_e)$, performed with Eq. (8) for the three noble metals, are shown in Figs. 2(d), 3(d), and 4(d). The common features of the three dependences are a nearly constant strength of the electron-phonon coupling up to the temperatures of ~3000 K for Cu and Au, and ~5000 K for Ag, and a significant strengthening of the electron-phonon coupling at higher temperatures when a large number of d electrons are thermally excited and contribute to the electron-phonon energy exchange. The rate and the degree of the increase of $G(T_e)$ with respect to the low-temperature levels, however, are different for the three metals and are defined by the detailed structures of the DOSs, particularly by the locations, the widths, and the shapes of the d bands. The d bands in Cu and Au are located at approximately the same depth under the Fermi level, but the width of the d band in Cu (~3.5 eV) is much smaller than the one in Au (~6 eV) [Figs. 3(a) and 4(a)]. This difference in the width of the d band is reflected in a higher density of states at the high-energy edge of the d band in Cu as compared to Au. As a result, for the same electron temperature, the thermal excitation of d band electrons in Cu leads to a more significant increase in the electron-phonon coupling factor as compared to Au, e.g., at $T_e = 10^4$ K, the electron-phonon coupling factor exceeds the room temperature value by a factor of 9.5 in Cu [Fig. 3(d)] compared to 5.8 in Au [Fig. 4(d)]. The widths of the d bands in Ag and Cu are similar, but the separation of the d band from the Fermi level is larger in Ag [Figs. 2(a) and 3(a)]. As a result, at the same electron temperature of 10^4 K, the electron-phonon coupling in Cu exceeds its room temperature value by a factor of 9.5, as compared to 4.6 in Ag. Moreover, $G(T_e)$ saturates at $T_e \geq 1.5 \times 10^4$ K in Cu, but continues a sharp rise at and above this temperature in Ag [Figs. 2(d) and 3(d)].

While the temperature dependences of the electron-phonon coupling calculated with Eq. (8) are defined mainly by the characteristics of the electron DOS, the low-temperature levels in these calculations are preset by the choice of the value of $\lambda\langle\omega^2\rangle$. For Ag, the calculations are performed with a value of $\lambda\langle\omega^2\rangle$ obtained using the approximation of $\langle\omega^2\rangle \approx \theta_D^2/2$ and λ evaluated from the experimental electrical resistivity data,[55] as shown in Table I. This estimation of $\lambda\langle\omega^2\rangle$ gives a relatively good agreement of the room temperature values of the electron-phonon

coupling factor predicted by Eq. (8), $G(300\ \mathrm{K})=2.5\times10^{16}\ \mathrm{W\ m^{-3}\ K^{-1}}$, with the experimental value of the electron-phonon coupling constant, $3.5\times10^{16}\ \mathrm{W\ m^{-3}\ K^{-1}}$, measured in femtosecond optical transient-reflection experiments performed at low laser excitations, when the increase of the electron temperature does not exceed 90 K.[56,57]

For Cu and Au, the values of $\lambda\langle\omega^2\rangle$ obtained in pump-probe reflectivity measurements, performed with laser excitations at which the electron temperature does not exceed 1000 K,[58] are used in the calculations (Table I). The levels of the low-temperature plateaus in the dependences $G(T_e)$ calculated for Cu and Au are in good agreement with the values of the electron-phonon coupling constants measured in pump-probe experiments, $(3.5–4.0)\times10^{16}\ \mathrm{W\ m^{-3}\ K^{-1}}$,[59] $3.0\times10^{16}\ \mathrm{W\ m^{-3}\ K^{-1}}$,[56] $2.9\times10^{16}\ \mathrm{W\ m^{-3}\ K^{-1}}$,[52] and $2.2\times10^{16}\ \mathrm{W\ m^{-3}\ K^{-1}}$ (Ref. 6) for Au, and $10^{17}\ \mathrm{W\ m^{-3}\ K^{-1}}$ (Refs. 6 and 60) for Cu. Note that all of these experiments are performed at relatively low laser excitations when the variation of the electron temperature is limited to the range of temperatures up to ~3000 K that corresponds to nearly constant values of the electron-phonon coupling factor [Figs. 3(d) and 4(d)].

At higher laser fluences, typical for laser processing applications, the temperature dependence of the electron-phonon coupling starts to play an important role in defining the characteristics of the material response to the laser excitation. The enhancement of the electron-phonon coupling at high electron temperatures implies a faster energy transfer from the hot electrons to the lattice, generation of stronger thermoelastic stresses, reduction of the threshold fluences for the onset of laser melting and ablation, as well as changes in the time scales of the laser-induced phase transformations. In particular, the results of recent TTM-MD simulations of femtosecond laser melting of 20 nm Au films[20] demonstrate that the time of the melting onset, measured in time-resolved electron diffraction experiments,[31,61] can only be reproduced with a model accounting for the temperature dependence of the electron-phonon coupling. A simulation performed with a constant electron-phonon coupling and a linear temperature dependence of the electron heat capacity is found to overpredict the time of the beginning of the melting process by a factor of 2. Similarly, an introduction of the temperature dependent electron-phonon coupling is found to be necessary in order to reconcile the calculated and experimental values of the ablation threshold and the fluence dependence of the ablation depth in Au films irradiated by 500 fs laser pulses,[33,35] as well as to provide a good computational description of electron photoemission data.[18,30,34]

In this study, no attempt has been made to account for the modifications in the electron DOS due to the changes of the electronic structure at elevated electron temperatures. Recent electronic structure calculations performed for Au and Al at an electron temperature of 6 eV (Ref. 62) predict that the reduced screening due to the thermal excitation of *d* band electrons results in a significant width compression and shift to lower energies of the *d* band in Au, whereas the Al electron DOS at 6 eV remains the same as the one at 0 K. Although the modifications of the electron DOS of Au at high electron temperatures would not affect the essential physics responsible for the temperature dependence of the electron heat capacity and electron-phonon coupling, they may introduce some quantitative corrections to these dependences and should be taken into account in a more detailed analysis of the material response to the extreme levels of laser excitation. In the range of electron temperatures considered in this work ($T_e\leq2$ eV), however, the effect of the modification of the electron DOS on the calculated thermophysical properties is expected to be relatively small.

C. Nickel and platinum

In transition metals with almost full *d* bands, such as Ni and Pt, the Fermi level cuts through the high-energy edge of the *d* bands [Figs. 5(a) and 6(a)], leading to a very high density of electron states at the Fermi level. The *d* band electrons at the energy levels around the Fermi energy can be easily excited even at low electron temperatures, shifting the Fermi level (chemical potential) to higher energies [Figs. 5(b) and 6(b)] and altering the electron heat capacity and the electron-phonon coupling in a way very different from what is discussed above for the free electron gas model, Al, and noble metals. Indeed, the excitation of electrons from the high density of states *d* band to the much lower density of states *s* band [Figs. 5(a) and 6(a)] and the shift of the chemical potential to higher energies, away from the high density of states edge of the *d* band [Figs. 5(b) and 6(b)], result in strong negative deviations of the heat capacity from the linear dependences, $C_e(T_e)=\gamma T_e$, shown in Figs. 5(c) and 6(c) for low-temperature experimental values of the coefficient γ [$1077.4\ \mathrm{J\ m^{-3}\ K^{-2}}$ for Ni and $748.1\ \mathrm{J\ m^{-3}\ K^{-2}}$ for Pt (Ref. 47)].

The trend of the negative deviation of the electron heat capacity from the linear dependence agrees with experimental results reported in Ref. 63 for Ni and Pt, where the electron heat capacity was obtained by subtracting the lattice heat capacity (assumed to follow the Dulong-Petit law at high temperatures) from the total heat capacity measured in experiments for temperatures up to 1600 K. The results of the calculations of the electron heat capacity of Pt, shown in Fig. 5(c), are also consistent with earlier calculations reported in Ref. 22.

The temperature dependences of the electron-phonon coupling are shown for Ni and Pt in Figs. 5(d) and 6(d). The values of $\lambda\langle\omega^2\rangle$, used in the calculations, are based on the values of the electron-phonon coupling constants measured in pump-probe reflectivity experiments, $10.5\times10^{17}\ \mathrm{W\ m^{-3}\ K^{-1}}$ for Ni and $10.9\times10^{17}\ \mathrm{W\ m^{-3}\ K^{-1}}$ for Pt.[37] Since the experiments were performed under low-excitation conditions, when the transient increase of the electron temperature above the room temperature did not exceed 100 K for Ni and 150 K for Pt, the measured coupling constants are taken here as the room temperature values and are used in Eq. (8) to obtain $\lambda\langle\omega^2\rangle$ listed in Table I. These values of $\lambda\langle\omega^2\rangle$ are relatively close to the estimations based on experimental measurements of λ and the approximation $\langle\omega^2\rangle\approx\theta_D^2/2$ (see Table I).

The temperature dependences of the electron-phonon coupling predicted for Ni and Pt are similar and are character-

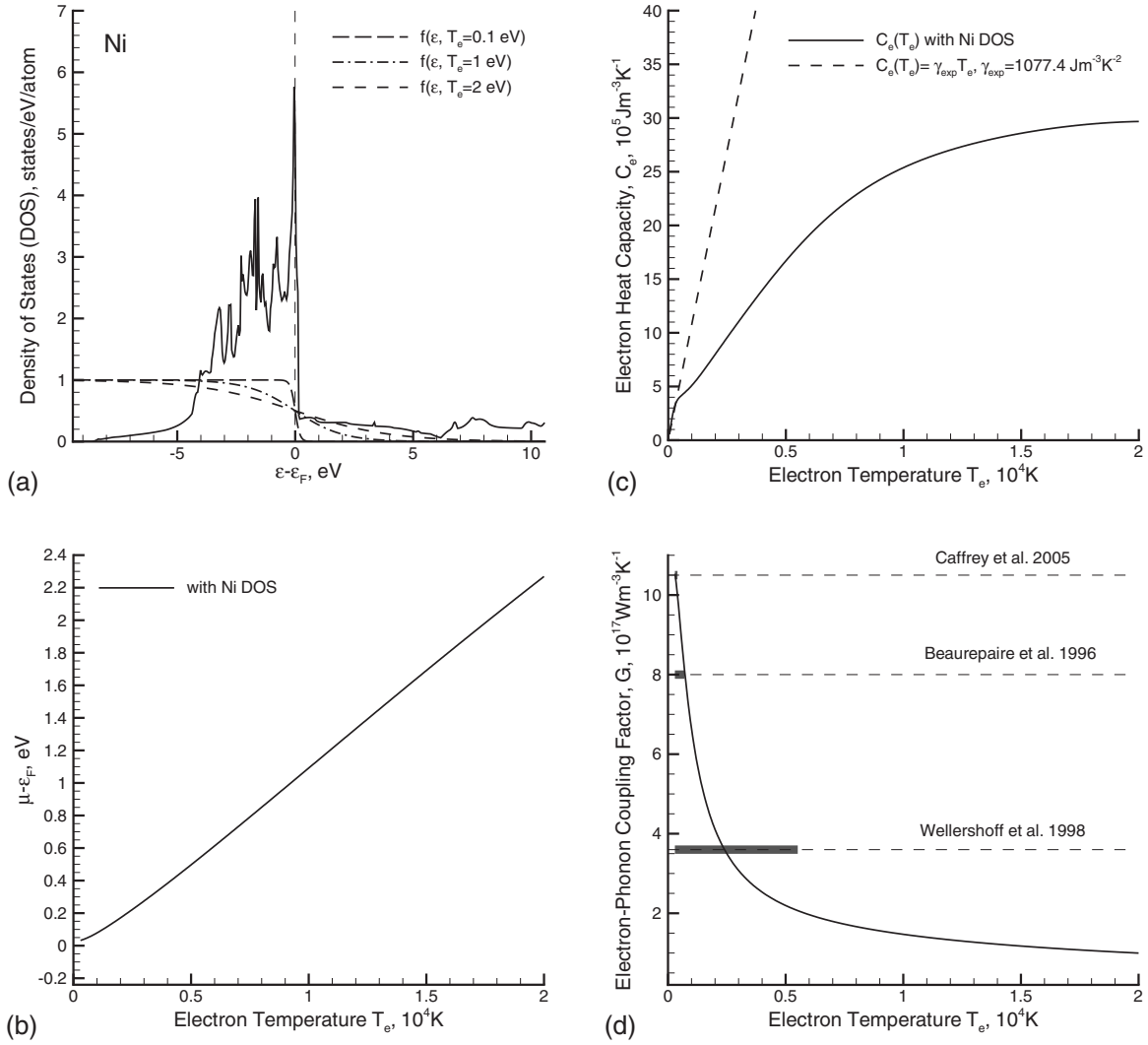

FIG. 5. Same as Fig. 2 but for nickel.

ized by a steep decrease as temperature increases up to $(3-5)\times 10^3$ K, followed by a slower decrease with further temperature rise. This temperature dependence can be explained based on the analysis of the electron DOS of the two transition metals [Figs. 5(a) and 6(a)]. Thermal excitation of *d* band electrons leads to the shift of the chemical potential to higher energies and away from the high density of states edge of the *d* band [Figs. 5(b) and 6(b)]. This shift reduces the contribution of the *d* band electrons to the electron-phonon coupling, with the reduction being particularly sharp as the temperature increases up to several thousand Kelvins, leading to the separation of the Fermi level from the edge of the *d* band. In particular, as the electron temperature increases up to 5000 K, the electron-phonon coupling drops, with respect to the room temperature values, by a factor of 4.8 for Ni and 2.8 for Pt. Further slower decrease of the electron-phonon coupling is defined by the balance between the increased probability of the thermal excitations from deeper energy levels and the continuing shift of the chemical potential to higher energies.

The reduction in the strength of the electron-phonon coupling with increasing electron temperature is consistent with the relative values of the electron-phonon coupling constants obtained in experiments performed at different levels of laser excitation. In particular, for Ni, the highest value of the electron-phonon constant, 10.5×10^{17} W m^{-3} K^{-1}, is measured in transient thermoreflectance experiments,[37] where the maximum electron temperature increase does not exceed 100 K. A somewhat smaller value of 8×10^{17} W m^{-3} K^{-1} is deduced from pump-probe transmission experiments,[38] where the electron temperature goes up to 700 K. Finally, the smallest value of the coupling constant, 3.6×10^{17} W m^{-3} K^{-1}, is obtained by fitting the predictions of the TTM calculations to the threshold fluences for the onset of surface melting.[39] The electron temperature in the latter case reaches several thousands of Kelvins and the reported value of the effective electron-phonon coupling "constant" is consistent with the temperature dependence shown in Fig. 5(d).

Large negative deviations of the electron heat capacity from the linear temperature dependence suggest that the commonly used linear temperature dependence may result in a significant underestimation of the transient values of the electron temperature during the time of the electron-phonon nonequilibrium in Ni and Pt targets. The fast drop of the

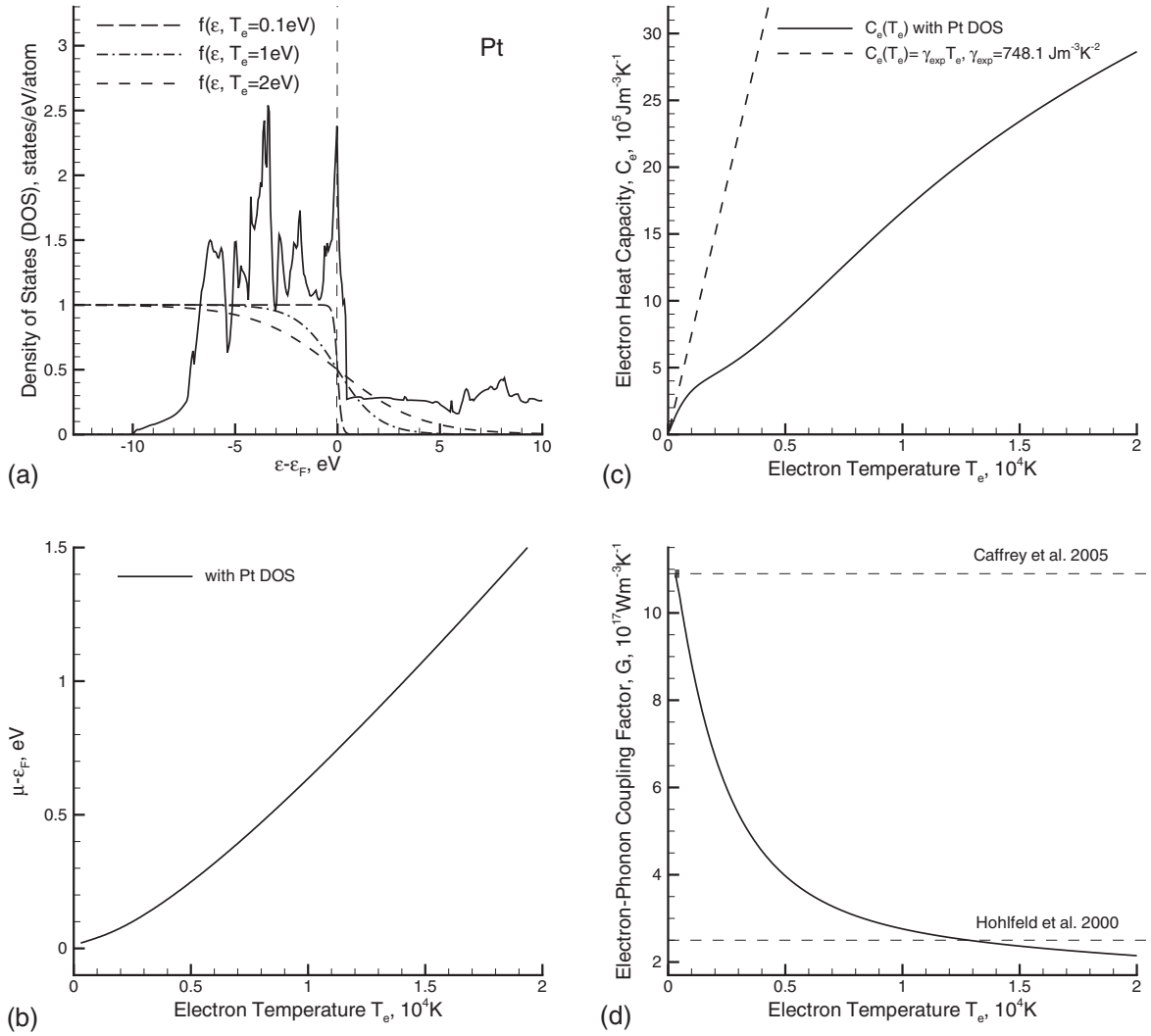

FIG. 6. Same as Fig. 2 but for platinum. The range of the electron temperature variation in the experiment used in the measurement of the electron-phonon coupling of Pt by Hohlfeld *et al.* is not given in Ref. 6 and, therefore, is not shown in (d).

strength of the electron-phonon coupling with increasing electron temperature, on the other hand, can slow down the electron-lattice energy equilibration and reduce the localization of the deposited laser energy in the surface region of the irradiated target. Incorporation of the modified temperature dependences into TTM or TTM-MD models may improve the reliability of the models in the quantitative analysis of practically important characteristics in laser processing applications. In particular, preliminary TTM calculations incorporating the modified temperature dependence of the thermophysical properties of Ni (Ref. 21) predict the threshold laser fluences for surface melting in films of different thicknesses that are closer to the experimentally measured values as compared to the results obtained with commonly used approximations of the thermophysical properties.

D. Tungsten and titanium

The last two metals considered in this paper are W and Ti, transition metals with bcc and hcp crystal structures, respectively. The characteristic feature of the electron DOS of these metals is a wide (~10 eV) less than half-filled *d* band with relatively small values of density of states at the Fermi level, located within a local dip in the DOS [Figs. 7(a) and 8(a)]. The complex structure of the DOS results in a complex and, in some cases, nonmonotonic temperature dependence of the thermophysical properties of these metals.

In tungsten, the region of thermal excitations ($\sim k_B T_e$) at low temperatures, below ~3000 K, has nearly the same density of states residing on both sides of the Fermi level [Fig. 7(a)], resulting in relatively small variations of the chemical potential [Fig. 7(b)] and the temperature dependence of the electron heat capacity following the linear dependence characteristic of the free electron gas model. At electron temperatures exceeding 3000 K, the temperature dependence of the electron heat capacity exhibits positive deviations from the linear dependence [Fig. 7(c)], similar to the ones predicted for noble metals [Figs. 2(c), 3(c), and 4(c)]. The split from the linear dependence in W, however, is not as drastic as in the case of the noble metals, with the maximum deviation observed at a temperature of 1.1×10^4 K, when the heat capacity exceeds the value predicted by the linear dependence

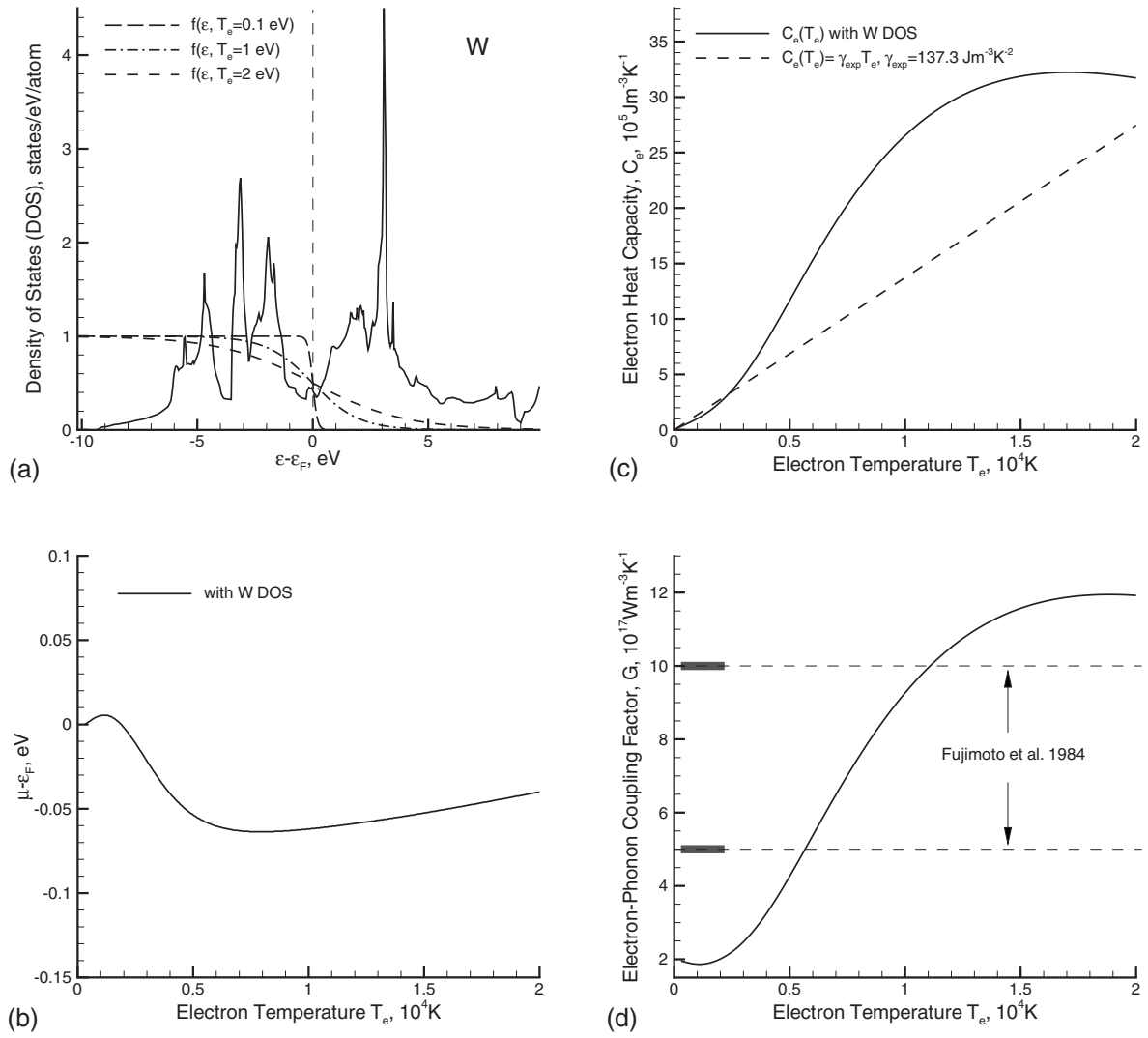

FIG. 7. Same as Fig. 2 but for tungsten.

by a factor of 1.9. At higher temperatures, the electron heat capacity saturates and even starts to decrease at $T_e \geqslant 1.7 \times 10^4$ K.

The comparison of the DOS of noble metals [Figs. 2(a), 3(a), and 4(a)] and tungsten [Fig. 7(a)] reveals that the high density of states peaks of the d band in W are closer to the Fermi level, which, unlike in the case of the noble metals, does not shift to higher energies with increasing electron temperature [compare Figs. 2(b), 3(b), and 4(b) with Fig. 7(b)]. Furthermore, the number of occupied d states in W is much smaller due to fewer $5d$ electrons in W as compared to the number of d electrons in the noble metals. As a result, the effective contribution of the presence of high density of d states on both sides of the Fermi level to the electron heat capacity of W diminishes at temperatures exceeding $\sim 1 \times 10^4$ K.

The characteristic features of the electron DOS of W discussed above also affect the temperature dependence of the electron-phonon coupling [Fig. 7(d)]. While a significant increase of the strength of the electron-phonon coupling is ensured by the high values of the density of states on both sides from the Fermi level, the coupling tends to saturate at $T_e \geqslant 1.5 \times 10^4$ K. This behavior can be related to the results obtained for Cu, whose d band is relatively close to the Fermi level and narrow in width [Fig. 3(d)]. Although, due to the larger number of d electrons, the increase in the electron-phonon coupling above the room temperature value is larger in Cu (11-fold increase in Cu vs sixfold increase in W at $T_e = 2 \times 10^4$ K), the overall shapes of the temperature dependences are similar for the two metals. Similar temperature dependences of the electron heat capacity and the electron-phonon coupling are also predicted for molybdenum,[53] which has the characteristics of the electron DOS similar to tungsten.

The predicted temperature dependence of the electron-phonon coupling for W can be related to the results of pump-probe photoemission measurements, suggesting that the value of the electron-phonon coupling constant is within the range of $(5-10) \times 10^{17}$ W m^{-3} K^{-1}.[64] Although these values are within the range of variation of the electron-phonon coupling predicted in this work [Fig. 7(d)], the electron temperature variations estimated for the laser excitations used in the pump-probe experiments are within several thousand Kelvins, where the coupling strength exhibits relatively weak

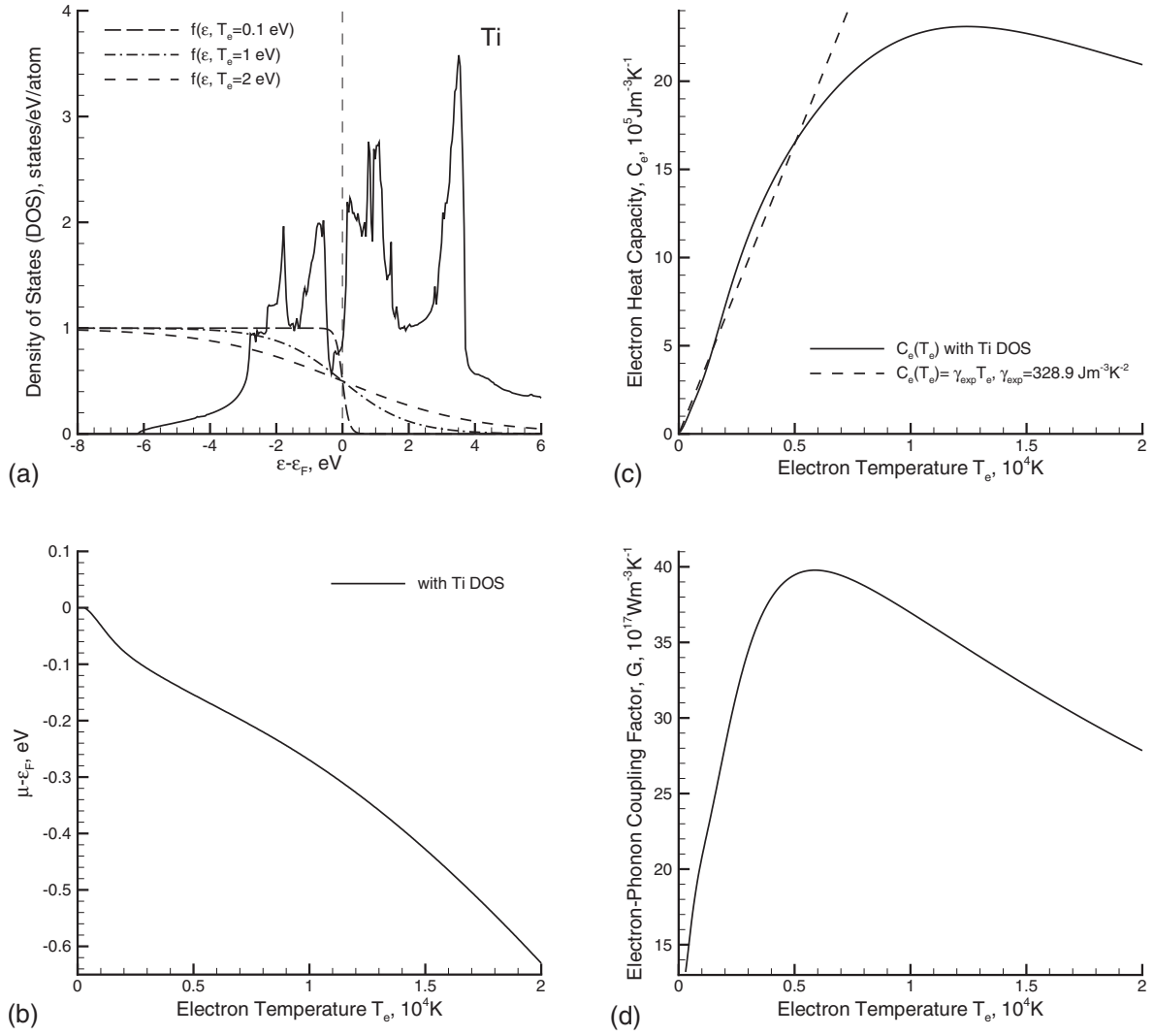

FIG. 8. Same as Fig. 2 but for titanium.

temperature dependence. The low-temperature value of $\lambda\langle\omega^2\rangle$, obtained in pump-probe reflectivity measurements[58] and used in the calculation of the temperature dependence shown in Fig. 7(d), yields a value of the coupling constant, 2×10^{17} W m^{-3} K^{-1}, that is outside the range suggested in Ref. 64. This discrepancy in the reported experimental values suggests that additional accurate measurements of the electron-phonon coupling at low excitation levels are needed to verify the position of the low-temperature level of the coupling strength in the dependence shown in Fig. 7(d).

A distinct characteristic of the electron DOS of titanium is the presence of a high density of available d states right above the Fermi level [Fig. 8(a)]. Thermal excitation of d electrons to the higher density of states energy region leads to a shift of the chemical potential to lower energies. The electron heat capacity, however, follows the linear dependence up to ~6000 K and exhibits a sharp turn from an almost linear increase to a decrease after reaching its maximum value at $\sim1.2\times10^4$ K. Similarly, the electron-phonon coupling shows a nonmonotonic temperature dependence, with a strong enhancement of the coupling strength at $T_e \leqslant 5000$ K, followed by a decrease at $T_e \geqslant 6000$ K.

An interpretation of the temperature dependences predicted for Ti can be provided based on the analysis of the contributions from the two high density of states regions present on both sides of the Fermi level, similar to the case of W discussed above. At a quantitative level, however, the transitions from the increase to the saturation and the decrease of both the electron heat capacity and the electron-phonon coupling take place within a much narrower electron temperature range in Ti, as compared to W. The differences in temperature sensitivity of the thermophysical properties of the two metals can be explained by the quantitative differences in their electron DOS. In particular, a smaller number of d electrons, a smaller width of the occupied part of the d band, and a large gap between two high-density peaks at ~1 and ~3.5 eV above the Fermi level are the factors that contribute to the higher temperature sensitivity of the electron heat capacity and the electron-phonon coupling in Ti, as compared to W.

For the electron-phonon coupling in titanium, a high value of 10^{19} W m^{-3} K^{-1} has been estimated from fitting the sputtering yields measured in heavy ion bombardment of Ti targets to the predictions of the inelastic thermal spike model.[3,65] This value is more than twice larger than the maxi-

mum value obtained in the present calculations [Fig. 8(d)]. Given the uncertainty with respect to an adequate representation of the sputtering mechanisms by the inelastic thermal spike model, however, the accuracy of the evaluation of the coupling constant in sputtering experiments is limited and the predicted value can be considered only as a rough estimate. The temperature dependence, shown in Fig. 8(d), is based on the value of $\lambda\langle\omega^2\rangle$, obtained in pump-probe reflectivity experiments[58] and corresponding to the room temperature electron-phonon coupling factor of 1.3×10^{18} W m^{-3} K^{-1}. While the low-temperature value of the electron-phonon coupling factor may require further verification in accurate pump-probe experiments, it is apparent, from the results of the calculations presented in this work, that the strong temperature dependences of the electron-phonon coupling and the electron heat capacity are the direct consequences of the characteristics of the electron DOS and should be taken into account in the interpretation of experimental data obtained under conditions when the transient values of the electron temperature undergo significant variations.

IV. SUMMARY

The connections between the electron DOS and the electron temperature dependences of the electron-phonon coupling and the electron heat capacity are investigated for eight representative metals (aluminum, copper, silver, gold, nickel, platinum, tungsten, and titanium). The electron DOSs used in the calculations of the thermophysical properties are obtained from *ab initio* electronic structure calculations performed within the density functional theory. The results of the calculations suggest that the effect of the thermal excitation of electrons on the thermophysical properties is sensitive to the structure of the electron DOS and can lead to large variations of the properties under conditions of electron-phonon nonequilibrium generated in the material by short-pulse laser irradiation or energetic ion bombardment.

For Al, the free electron gas model provides a good description of the temperature dependence of the electron heat capacity, but fails to predict a relatively moderate ($\sim$40%) increase in the strength of the electron-phonon coupling with increasing electron temperature. In noble metals (Au, Cu, and Ag), the electron heat capacity and the electron-phonon coupling factor are strongly enhanced by the thermal excitation of *d* band electrons at electron temperatures exceeding several thousand Kelvins. In Ni and Pt, on the other hand, the location of the Fermi level at the high density of states edge of the *d* band results in the opposite trend when the thermal excitation of *d* band electrons leads to a drastic decrease in the electron-phonon coupling factor and large negative deviations of the electron heat capacity from the linear dependence on the electron temperature. For W and Ti, the location of the Fermi level in the middle of a partially filled *d* band, in a local dip in the electron DOS, results in complex nonmonotonic dependences of the thermophysical properties on the electron temperature.

Thus, depending on the electronic structure of a metal, the electron heat capacity and the electron-phonon coupling factor can increase, decrease, or exhibit nonmonotonic changes in response to the increase of the electron temperature. The range of electron temperatures considered in this work, up to 2×10^4 K, is typical for the electron temperature variations in ultrafast laser materials processing applications. The strong deviations of the thermophysical properties from the commonly used approximations of a constant electron-phonon coupling and a linear dependence of the electron heat capacity, revealed in this work, have important implications for quantitative computational analysis of ultrafast processes associated with laser interaction with metals. A number of practically important characteristics of the laser-material interaction, such as the threshold fluences for the onset of melting and ablation, the strength of the laser-induced stress wave, the emission of electrons from the irradiated surface, and the depth of the melting and/or heat-affected zone, can all be significantly altered by the transient changes of the thermophysical properties of the material occurring during the time of electron-phonon equilibration.

APPENDIX

For the completeness of the discussion of the electron-phonon coupling, presented in Sec. II D, the derivation of the equation for the temperature dependence of the electron-phonon coupling [Eq. (8)], not explicitly shown by Wang *et al.* in Ref. 18, is given in this appendix. The approximations used in the derivation are discussed, and the results obtained with the approximate Eq. (8) are compared with predictions of the full integration treatment of the energy exchange rate between the electrons and the phonons.

The expression for the electron-phonon energy exchange rate in Eq. (6) can be rewritten as

$$\left.\frac{\partial E_e}{\partial t}\right|_{ep} = 2\pi g(\varepsilon_F)\int_0^\infty d\Omega\hbar\Omega\int_{-\infty}^\infty d\varepsilon\int_{-\infty}^\infty d\varepsilon'\,\alpha^2F(\varepsilon,\varepsilon',\Omega) \times S(\varepsilon,\varepsilon')\delta(\varepsilon-\varepsilon'+\hbar\Omega), \tag{A1}$$

where $S(\varepsilon,\varepsilon')=[f(\varepsilon)-f(\varepsilon')]n(\hbar\Omega,T_l)-f(\varepsilon')[1-f(\varepsilon)]$, and $f(\varepsilon)$ and $n(\hbar\Omega,T_l)$ denote the Fermi-Dirac and Bose-Einstein distribution functions, respectively: $f(\varepsilon)=1/\{1+\exp[(\varepsilon-\mu)/k_BT_e]\}$ and $n(\hbar\Omega,T_l)=1/[\exp(\hbar\Omega/k_BT_l)-1]$. It is convenient to rewrite the thermal factor as

$$S(\varepsilon,\varepsilon') = [f(\varepsilon)-f(\varepsilon')]\left\{n(\hbar\Omega,T_l)-\frac{f(\varepsilon')[1-f(\varepsilon)]}{f(\varepsilon)-f(\varepsilon')}\right\} = [f(\varepsilon)-f(\varepsilon')][n(\hbar\Omega,T_l)-n(\varepsilon'-\varepsilon,T_e)]. \tag{A2}$$

From the conservation of the total energy in the electron-phonon scattering processes, i.e., $\varepsilon'=\varepsilon+\hbar\Omega$, one can simplify Eq. (A1) by eliminating the integration over ε'. Further, under the experimental conditions characteristic of laser processing, the high-temperature approximations ($\hbar\Omega \ll k_BT_e, \hbar\Omega \ll k_BT_l$) of the Bose-Einstein distribution functions present in Eq. (A2) can be used. Then, Eq. (A1) takes the following form:

$$\left.\frac{\partial E_e}{\partial t}\right|_{ep} = 2\pi g(\varepsilon_F)k_B(T_l - T_e)\int_0^\infty d\Omega \int_{-\infty}^{\infty} d\varepsilon \times \alpha^2F(\varepsilon, \varepsilon+\hbar\Omega, \Omega)[f(\varepsilon) - f(\varepsilon+\hbar\Omega)]. \quad \text{(A3)}$$

Using the assumption that $|M_{kk'}|^2$, when averaged over scattering angles, is independent of the electron states, the electron-phonon spectral function can be approximated as,[18] $\alpha^2F(\varepsilon,\varepsilon+\hbar\Omega,\Omega)=[g(\varepsilon)g(\varepsilon+\hbar\Omega)/g^2(\varepsilon_F)]\alpha^2F(\varepsilon_F,\varepsilon_F,\Omega)$. This approximation provides a simple description of the electron energy dependence of the Eliashberg spectral function based on the electron DOS. More sophisticated representations of the spectral function for different excited electron transitions, such as *ab initio* calculations using the linear-response approach,[66] have a potential for more accurate description of the temperature dependence of the electron-phonon coupling without making the assumption of the independence of the electron-phonon scattering matrix elements on the electron states. A more detailed consideration of the spectral function may introduce additional corrections to the temperature dependence of the electron-phonon coupling predicted in this work.

The approximate expression of the electron-phonon spectral function discussed above can be further simplified by assuming that $g(\varepsilon+\hbar\Omega)\sim g(\varepsilon)$, since ε varies in a much wider range (on the order of eV) than $\hbar\Omega$ ($\sim$50 meV, defined by the Debye frequency). Then, Eq. (A3) can be rewritten as

$$\left.\frac{\partial E_e}{\partial t}\right|_{ep} = 2\pi\hbar g(\varepsilon_F)k_B(T_l - T_e) \times \int_0^\infty d\Omega \alpha^2F(\Omega)\Omega \int_{-\infty}^{\infty} d\varepsilon \frac{g(\varepsilon)^2}{g(\varepsilon_F)^2}\left(-\frac{\partial f}{\partial \varepsilon}\right). \quad \text{(A4)}$$

Expressing the integral over phonon frequencies through $\lambda\langle\omega^2\rangle$, defined in Sec. II D, and introducing the temperature dependent electron-phonon coupling factor through $\partial E_e/\partial t|_{ep}=G(T_e)(T_l-T_e)$, one can arrive at the expression for $G(T_e)$ given by Eq. (8).

Alternatively, one can obtain $G(T_e)$ without making an assumption of $g(\varepsilon+\hbar\Omega)\sim g(\varepsilon)$ as well as without using the high-temperature approximations of the Bose-Einstein distribution functions in the derivation of Eq. (A4). This can be done by a straightforward numerical calculation of the rate of the electron-phonon energy exchange $\partial E_e/\partial t$ directly from Eq. (A1) while retaining the description of the electron energy dependence of the electron-phonon spectral function based on the electron DOS.

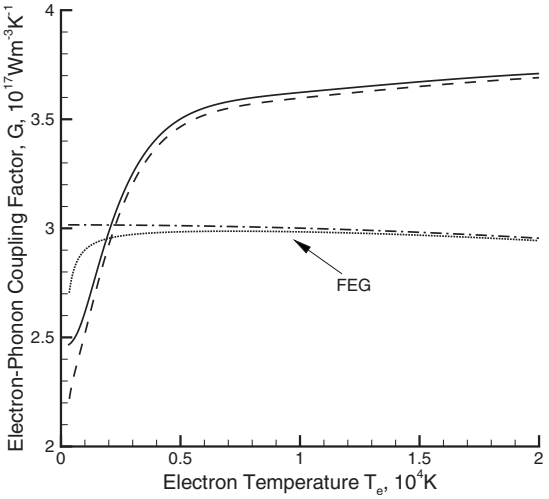

FIG. 9. Temperature dependence of the electron-phonon coupling factor calculated with aluminum (solid and dashed lines) and the free electron gas model (dash-dotted and dotted lines) electron DOS using Eq. (8) (solid and dash-dotted lines) and Eq. (A5) (dashed and dotted lines). The results obtained with Eq. (A5) are normalized so that $\lambda\langle\omega^2\rangle$ calculated from $\alpha^2F(\Omega)$ has the same value as the one used in Eq. (8), i.e., 185.9 meV^2 shown for aluminum in Table I.

The temperature dependent electron-phonon coupling can then be directly related to the rate of the energy exchange between the electrons and the lattice:

$$G(T_e) = \frac{2\pi\hbar g(\varepsilon_F)}{T_l - T_e}\int_0^\infty d\Omega\alpha^2F(\Omega)\Omega\int_{-\infty}^{\infty} d\varepsilon \frac{g(\varepsilon)g(\varepsilon+\hbar\Omega)}{g(\varepsilon_F)^2} \times S(\varepsilon,\varepsilon+\hbar\Omega). \quad \text{(A5)}$$

In order to evaluate the assumptions made in the derivation of Eq. (8), the temperature dependence of the electron-phonon coupling is calculated for aluminum at T_l=300 K with both theoretical approaches, i.e., Eqs. (8) and (A5). The spectral function $\alpha^2F(\Omega)$ obtained in *ab initio* linear-response calculations for aluminum[50] is used in Eq. (A5), and the electron DOSs of the free electron gas model and aluminum are used in both calculations. The comparison of the results obtained with the two approaches, shown in Fig. 9, suggests that the approximation of $g(\varepsilon+\hbar\Omega)\sim g(\varepsilon)$ has a negligible effect on the temperature dependence of the calculated coupling factor, whereas the increasing deviation between the predictions of the two methods at low T_e can be related to the high-temperature approximations of the Bose-Einstein distribution functions used in the derivation of Eq. (8). Additional calculations of $G(T_e)$ for other metals performed with Eq. (A5) also show similarly small deviations from the results obtained with Eq. (8).

*lz2n@virginia.edu;
URL: http://www.faculty.virginia.edu/CompMat/

[1] S. I. Anisimov, B. L. Kapeliovich, and T. L. Perel'man, Zh. Eksp. Teor. Fiz. **66**, 776 (1974) [Sov. Phys. JETP **39**, 375 (1974)].
[2] Z. G. Wang, Ch. Dufour, E. Paumier, and M. Toulemonde, J. Phys.: Condens. Matter **6**, 6733 (1994).
[3] M. Toulemonde, W. Assmann, C. Trautmann, F. Grüner, H. D. Mieskes, H. Kucal, and Z. G. Wang, Nucl. Instrum. Methods

Phys. Res. B **212**, 346 (2003).
[4] T. Q. Qiu and C. L. Tien, J. Heat Transfer **115**, 842 (1993).
[5] P. E. Hopkins and P. M. Norris, Appl. Surf. Sci. **253**, 6289 (2007).
[6] J. Hohlfeld, S.-S. Wellershoff, J. Güdde, U. Conrad, V. Jähnke, and E. Matthias, Chem. Phys. **251**, 237 (2000).
[7] J. K. Chen and J. E. Beraun, Numer. Heat Transfer, Part A **40**, 1 (2001).
[8] J. K. Chen, J. E. Beraun, L. E. Grimes, and D. Y. Tzou, Int. J. Solids Struct. **39**, 3199 (2002).
[9] E. Carpene, Phys. Rev. B **74**, 024301 (2006).
[10] H. Hakkinen and U. Landman, Phys. Rev. Lett. **71**, 1023 (1993).
[11] C. Schäfer, H. M. Urbassek, and L. V. Zhigilei, Phys. Rev. B **66**, 115404 (2002).
[12] D. S. Ivanov and L. V. Zhigilei, Phys. Rev. B **68**, 064114 (2003).
[13] E. Leveugle, D. S. Ivanov, and L. V. Zhigilei, Appl. Phys. A: Mater. Sci. Process. **79**, 1643 (2004).
[14] Z. Lin and L. V. Zhigilei, Phys. Rev. B **73**, 184113 (2006).
[15] C. Cheng and X. Xu, Phys. Rev. B **72**, 165415 (2005).
[16] F. Gao, D. J. Bacon, P. E. J. Flewitt, and T. A. Lewis, Modell. Simul. Mater. Sci. Eng. **6**, 543 (1998).
[17] D. M. Duffy and A. M. Rutherford, J. Phys.: Condens. Matter **19**, 016207 (2007).
[18] X. Y. Wang, D. M. Riffe, Y. S. Lee, and M. C. Downer, Phys. Rev. B **50**, 8016 (1994).
[19] A. N. Smith and P. M. Norris, Proceedings of the 11th International Heat Transfer Conference, 1998 (Korean Society of Mechanical Engineers, 1998), Vol. 5, p. 241.
[20] Z. Lin and L. V. Zhigilei, Proc. SPIE **6261**, 62610U (2006).
[21] Z. Lin and L. V. Zhigilei, Appl. Surf. Sci. **253**, 6295 (2007).
[22] T. Tsuchiya and K. Kawamura, Phys. Rev. B **66**, 094115 (2002).
[23] G. Kresse and J. Hafner, Phys. Rev. B **47**, 558 (1993); **49**, 14251 (1994).
[24] G. Kresse and D. Joubert, Phys. Rev. B **59**, 1758 (1999).
[25] H. J. Monkhorst and J. D. Pack, Phys. Rev. B **13**, 5188 (1976).
[26] A. E. Mattsson, P. A. Schultz, M. P. Desjarlais, T. R. Mattsson, and K. Leung, Modell. Simul. Mater. Sci. Eng. **13**, R1 (2005).
[27] N. W. Ashcroft and N. D. Mermin, *Solid State Physics* (Holt, Rinehart and Winston, New York, 1976).
[28] M. Kaveh and N. Wiser, Adv. Phys. **33**, 257 (1984).
[29] M. I. Kaganov, I. M. Lifshitz, and L. V. Tanatarov, Zh. Eksp. Teor. Fiz. **31**, 232 (1956) [Sov. Phys. JETP **4**, 173 (1957)].
[30] W. S. Fann, R. Storz, H. W. K. Tom, and J. Bokor, Phys. Rev. Lett. **68**, 2834 (1992).
[31] J. R. Dwyer, R. E. Jordan, C. T. Hebeisen, M. Harb, R. Ernstorfer, T. Dartigalongue, and R. J. D. Miller, J. Mod. Opt. **54**, 905 (2007).
[32] O. P. Uteza, E. G. Gamaly, A. V. Rode, M. Samoc, and B. Luther-Davies, Phys. Rev. B **70**, 054108 (2004).
[33] J. K. Chen and J. E. Beraun, J. Opt. A, Pure Appl. Opt. **5**, 168 (2003).
[34] J. P. Girardeau-Montaut and C. Girardeau-Montaut, Phys. Rev. B **51**, 13560 (1995).
[35] J. K. Chen, W. P. Latham, and J. E. Beraun, J. Laser Appl. **17**, 63 (2005).
[36] B. H. Christensen, K. Vestentoft, and P. Balling, Appl. Surf. Sci. **253**, 6347 (2007).
[37] A. P. Caffrey, P. E. Hopkins, J. M. Klopf, and P. M. Norris, Microscale Thermophys. Eng. **9**, 365 (2005).
[38] E. Beaurepaire, J.-C. Merle, A. Daunois, and J.-Y. Bigot, Phys. Rev. Lett. **76**, 4250 (1996).
[39] S.-S. Wellershoff, J. Güdde, J. Hohlfeld, J. G. Müller, and E. Matthias, Proc. SPIE **3343**, 378 (1998).
[40] D. Y. Tzou, *Macro- to Microscale Heat Transfer: The Lagging Behavior* (Taylor & Francis, Washington, DC, 1997).
[41] P. B. Allen, Phys. Rev. Lett. **59**, 1460 (1987).
[42] J. M. Ziman, *Electrons and Phonons* (Oxford University Press, London, 1960).
[43] W. L. McMillan, Phys. Rev. **167**, 331 (1968).
[44] G. Grimvall, in *The Electron-Phonon Interaction in Metals*, edited by E. Wohlfarth, Selected Topics in Solid State Physics (North-Holland, New York, 1981).
[45] E. V. Chulkov, A. G. Borisov, J. P. Gauyacq, D. Sánchez-Portal, V. M. Silkin, V. P. Zhukov, and P. M. Echenique, Chem. Rev. (Washington, D.C.) **106**, 4160 (2006), and references therein.
[46] Yu. V. Petrov, Laser Part. Beams **23**, 283 (2005).
[47] *American Institute of Physics Handbook*, 3rd ed. (McGraw-Hill, New York, 1972).
[48] N. E. Phillips, Phys. Rev. **114**, 676 (1959).
[49] R. Bauer, A. Schmid, P. Pavone, and D. Strauch, Phys. Rev. B **57**, 11276 (1998).
[50] S. Y. Savrasov and D. Y. Savrasov, Phys. Rev. B **54**, 16487 (1996).
[51] D. A. Papaconstantopoulos, L. L. Boyer, B. M. Klein, A. R. Williams, V. L. Morruzzi, and J. F. Janak, Phys. Rev. B **15**, 4221 (1977).
[52] J. L. Hostetler, A. N. Smith, D. M. Czajkowsky, and P. M. Norris, Appl. Opt. **38**, 3614 (1999).
[53] Electron temperature dependences of thermophysical properties of metals discussed in this paper are accessible in tabulated form from http://www.faculty.virginia.edu/CompMat/electron-phonon-coupling/
[54] B. Rethfeld, A. Kaiser, M. Vicanek, and G. Simon, Phys. Rev. B **65**, 214303 (2002).
[55] P. B. Allen, Phys. Rev. B **36**, 2920 (1987).
[56] R. H. M. Groeneveld, R. Sprik, and A. Lagendijk, Phys. Rev. B **51**, 11433 (1995).
[57] R. H. M. Groeneveld, R. Sprik, and A. Lagendijk, Phys. Rev. Lett. **64**, 784 (1990).
[58] S. D. Brorson, A. Kazeroonian, J. S. Moodera, D. W. Face, T. K. Cheng, E. P. Ippen, M. S. Dresselhaus, and G. Dresselhaus, Phys. Rev. Lett. **64**, 2172 (1990).
[59] H. E. Elsayed-Ali, T. Juhasz, G. O. Smith, and W. E. Bron, Phys. Rev. B **43**, 4488 (1991).
[60] H. E. Elsayed-Ali, T. B. Norris, M. A. Pessot, and G. A. Mourou, Phys. Rev. Lett. **58**, 1212 (1987).
[61] J. R. Dwyer, C. T. Hebeisen, R. Ernstorfer, M. Harb, V. Deyirmenjian, R. E. Jordan, and R. J. D. Miller, Philos. Trans. R. Soc. London, Ser. A **364**, 741 (2006).
[62] V. Recoules, J. Clérouin, G. Zérah, P. M. Anglade, and S. Mazevet, Phys. Rev. Lett. **96**, 055503 (2006).
[63] G. K. White, Aust. J. Phys. **46**, 707 (1993).
[64] J. G. Fujimoto, J. M. Liu, E. P. Ippen, and N. Bloembergen, Phys. Rev. Lett. **53**, 1837 (1984).
[65] Ch. Dufour, E. Paumier, and M. Toulemonde, Nucl. Instrum. Methods Phys. Res. B **122**, 445 (1997).
[66] I. Y. Sklyadneva, A. Leonardo, P. M. Echenique, S. V. Eremeev, and E. V. Chulkov, J. Phys.: Condens. Matter **18**, 7923 (2006).